Correlations of Structure and Electronic Properties from EPR Spectroscopy of Hydroxylamine Oxidoreductase

Michael P. Hendrich,*,† Doros Petasis,†,§ David M. Arciero,‡ and Alan B. Hooper‡

Contributions from the Department of Chemistry, Carnegie Mellon University, Pittsburgh, Pennsylvania 15213, and the Department of Biochemistry, Molecular Biology and Biophysics, University of Minnesota, St. Paul, Minnesota 55108

Received August 10, 2000. Revised Manuscript Received February 2, 2001

Abstract: Hydroxylamine oxidoreductase (HAO) from the autotrophic nitrifying bacterium *Nitrosomonas europaea* catalyzes the oxidation of NH_2OH to HNO_2. The enzyme contains eight hemes per subunit which participate in catalytic function and electron transport. The structure of the enzyme shows a unique spatial arrangement of the eight hemes, subsets of which are now observed in four other proteins. The spatial arrangement displays three types of diheme pairing motifs. At least four of the eight hemes are electronically coupled in two distinguishable pairs and one of these pairs is at the active site of the enzyme. Here, the use of quantitative simulation of the EPR signals allows determination of exchange couplings, and assignments of signals and reduction potentials to hemes of the crystal structure. The absence of any obvious heme-to-heme bonding pathway in the crystal structure suggests that the observed exchange interactions are derived from direct electronic overlap of porphyrin orbitals. This provides evidence for heme pairs which function as biological two-electron redox centers in electron-transfer processes.

Introduction

The autotrophic bacterium, *Nitrosomonas europaea*, derives energy for growth from the oxidation of ammonia to nitrite. The pathway for this process contains two enzymes, ammonia monooxygenase (AMO) and hydroxylamine oxidoreductase (HAO).[1] AMO is a membrane-bound enzyme that catalyses the oxidation of ammonia in the reaction $NH_3 + O_2 + 2e^- + 2H^+ \rightarrow NH_2OH + H_2O$. HAO, a soluble enzyme found in the periplasmic region of the bacterium, catalyzes the reaction $NH_2OH + H_2O \rightarrow HNO_2 + 4e^- + 4H^+$.[2,3] The reducing equivalents generated in this reaction are the starting point for essential electron-transfer processes leading to ATP synthesis, reverse electron flow to $NADP^+$, and return of electrons to the primary monooxygenase reaction. HAO is a trimer of polypeptides with each monomer (68 kDa)[4] containing eight hemes covalently bound via two cysteine thioether linkages in the CXYCH sequences, for a total of 24 hemes per protein.[5] Seven of these are *c*-type hemes, while the eighth is an unusual prosthetic group, termed heme P460, which displays a Soret band at 463 nm for the reduced form of HAO. Six of the *c*-hemes have α-band absorption maxima at 553 nm in the ferrous form. These have midpoint redox potential values at +288, −10, −162, −192, −265, and −412 mV (vs NHE at pH 7).[6] The midpoint potentials for the seventh *c*-heme, which has an α-band at 559 nm, and the heme P460 are at +11 and −260 mV, respectively.

The function of the *c*-hemes is believed to be the transfer of electrons from the catalytic site to the binding site of the electron acceptor protein cytochrome c_{554}.[7,8] Several observations indicate that heme P460 is a component of the active site of HAO. Treatment of oxidized HAO with H_2O_2 causes loss of hydroxylamine reactivity and concomitant irreversible loss of the absorbency of ferrous P460, whereas the optical spectra of the *c*-hemes are unaffected.[9] An integer-spin EPR signal that originates from heme P460 vanishes in the presence of both substrates and cyanide.[10] Formation of the cyanide−HAO complex results in noncompetitive inhibition of hydroxylamine oxidation, inhibition of the reaction of ferric HAO with H_2O_2, and inhibition of the inactivation of HAO by organohydrazine suicide substrates.[11]

Heme P460 of HAO appears to be derived from a *c*-heme with typical covalent thioether linkages to Cys229 and Cys232, but also possesses a unique third covalent linkage between the 5-*meso* carbon of the porphyrin and the C3 ring carbon of Tyr467.[12,13] The tyrosine is from the polypeptide chain of a different monomeric subunit and is a cross-link between subunits. The novel structure of heme P460 may be responsible

* Address correspondence to this author. Phone: 412-268-1058. Fax: 412-268-1061. E-mail: hendrich@andrew.cmu.edu.

† Carnegie Mellon University.

§ Present address: Department of Physics, Allegheny College.

‡ University of Minnesota.

(1) Abbreviations: AMO, ammonia monooxygenase; HAO, hydroxylamine oxidoreductase.

(2) Hooper, A. B.; Nason, A. *J. Biol. Chem.* **1965**, *240*, 4044−4057.

(3) Andersson, K. K.; Hooper, A. B. *FEBS Lett.* **1983**, *164*, 236−240.

(4) Terry, K.; Hooper, A. B. *Biochemistry* **1981**, *20*, 7026−7032.

(5) Arciero, D. M.; Hooper, A. B. *J. Biol. Chem.* **1993**, *268*, 14645−14654.

(6) Collins, M.; Arciero, D. M.; Hooper, A. B. *J. Biol. Chem.* **1993**, *268*, 14655−14662.

(7) Hooper, A. B. In *Autotrophic Bacteria*; Schlegel, H. G., Bowien, B., Eds.; Science Tech Publishers: Madison, WI, 1989; pp 239−265.

(8) Arciero, D. M.; Balny, C.; Hooper, A. B. *Biochemistry* **1991**, *30*, 11466−11472.

(9) Hooper, A. B.; Terry, K. R. *Biochemistry* **1977**, *16*, 455−459.

(10) Hendrich, M. P.; Logan, M.; Andersson, K. K.; Arciero, D. M.; Lipscomb, J. D.; Hooper A. B. *J. Am. Chem. Soc.* **1994**, *116*, 11961−11968.

(11) (a) Logan, M. S. P.; Balny, C.; Hooper, A. B. *Biochemistry* **1995**, *34*, 9028−9037. (b) Logan, M. S. P.; Hooper, A. B. *Biochemistry* **1995**, *34*, 9257−9264.

(12) Igarashi, N.; Moriyama, H.; Fujiwara, T.; Fukumori, Y.; Tanaka, N. *Nat. Struct. Biol.* **1997**, *4*, 276−284.

(13) Arciero, D. M.; Hooper, A. B.; Cai, M.; Timkovich, R. *Biochemistry* **1993**, *32*, 9370−9378.

10.1021/ja002982d CCC: $20.00
Published on Web 03/13/2001

for its unusual electronic properties. Mössbauer spectroscopy of fully reduced HAO shows ferrous P460 to be high spin and to exhibit an unusually large quadrupole splitting ($\Delta E_Q = 4.21$ mm/s), thus the iron atom experiences the largest electric field gradient of any known naturally occurring ferrous heme.[14] Resonance Raman spectroscopy of ferrous P460 confirms that the band at 463 nm is a Soret band and that it is a unique heme with symmetry lower than those of protoporphyrin IX or chlorins.[15]

The EPR spectra of HAO are complicated by the sheer number of heme centers and by electronic interactions between various hemes. Here we show quantitative simulations of multifrequency EPR data from HAO, which allow deconvolution of the signals and determination of exchange interactions between heme pairs. From an analysis of the heme geometries of the crystal structure, we are able to make some assignments of EPR signals, with known reduction potentials, to corresponding hemes in the crystal structure.

The structure of HAO does not show reasonably close axial or peripheral bonds between any heme pair. Thus, the observed exchange interactions between the heme irons are believed to be mediated through overlap of porphyrin orbitals. This electronic interaction between heme pairs appears to be a novel function in heme proteins where the heme pairs function as two-electron redox centers.

Materials and Methods

Purification of Enzyme. Growth of *N. europaea* and purification of HAO were as described previously.[8,11] All experiments were performed in 50 mM potassium phosphate buffer, pH 7.5, unless otherwise noted. The concentration of HAO was determined spectrophotometrically for the oxidized state ($\epsilon = 700$ mM^{-1} cm^{-1} at 408 nm) and is given in terms of the subunit concentration (68 kDa) throughout this paper. The amount of P460 in HAO was determined from the difference spectrum of [reduced HAO plus CO] − [reduced HAO] ($\Delta\epsilon = 76$ mM^{-1} cm^{-1} for $A_{442} - A_{464}$).[11] Optical spectra were recorded with a HP spectrophotometer. For the EPR samples used in spin quantitation, accuracy of the extinction coefficients were checked by submitting aliquots for quantitative amino acid analysis. Extinction coefficients were found to be in agreement with previous determinations. All chemicals were reagent grade or better. Double distilled or Millipore Super Q water was used throughout.

EPR Spectroscopy. The X-band (9 GHz) EPR spectra were recorded on a Bruker 300 spectrometer equipped with an Oxford ESR-910 liquid helium cryostat and a Bruker bimodal cavity. The Q-band (35 GHz) EPR spectra were recorded on a Bruker 200 spectrometer with a home-built microwave cavity and immersion liquid helium cryostat.[16] The quantification of all X- and Q-band signals is relative to a CuEDTA spin standard. Unless otherwise stated, the spectra were obtained with field modulation of 1 mT_{pp} at 100 kHz. The magnetic field was calibrated with an NMR gaussmeter and the microwave frequency was measured with a counter. The S-band (3 GHz) spectra where collected at the National Biomedical ESR Center in the Medical College of Wisconsin. The spectra were recorded on a Varian spectrometer with a homemade microwave bridge and cavity, and an Air Products liquid helium cryostat. The P-band (14 GHz) spectra were collected at the Biophysical Research Division of the University of Michigan. The spectra were recorded on a homemade spectrometer with a Air Products liquid helium cryostat.

Analysis of EPR Spectra. The interpretation of the EPR spectra assumes the following spin Hamiltonian,

$$H_S = J\mathbf{S_1}\cdot\mathbf{S_2} + \mathbf{S_1}\cdot\mathbf{D'}\cdot\mathbf{S_2} + \mathbf{d}\cdot\mathbf{S_1}\times\mathbf{S_2} + \beta\mathbf{B}\cdot\mathbf{g_1}\cdot\mathbf{S_1} + \beta\mathbf{B}\cdot\mathbf{g_2}\cdot\mathbf{S_2} \quad (1)$$

The first three terms are from the common decomposition of the general exchange Hamiltonian,[17] where J is the isotropic exchange coupling between two low-spin heme centers ($S_1 = S_2 = {}^1/_2$), $\mathbf{D'}$ is a symmetric traceless tensor, and $\mathbf{d}$ is a polar vector of the antisymmetric contribution. For the last two terms in eq 1, $\mathbf{g_1}$ and $\mathbf{g_2}$ are the intrinsic $\mathbf{g}$-tensors of two hemes. The calculations for a monomeric heme use only one $\mathbf{g}$-tensor and the exchange terms are absent. Simulations of the EPR spectra are calculated from diagonalization of eq 1 with software created by the authors. The powder pattern is generated for a uniform spherical distribution of the magnetic field vector $\mathbf{B}$. The transition intensities are calculated from Fermi's Golden rule using the eigenfunctions given by diagonalization of eq 1 at the resonance condition. The spectral line width is dominated by g-strain and simulations use distributions of the g-values to give the correct line width. The distribution is specified as a σ_g-tensor where each component of the tensor is one standard deviation for a principal axis direction. Gaussian spin-packets of field width determined by the σ_g-tensor, and properly normalized for field-swept spectra, are folded into the spectrum at each calculated resonance field position. Least-squares and deconvolution analysis of the spectra are combined to allow relevant parameters to vary while maintaining a sum of multiple species which best fits the experimental data. The $\mathbf{g_2}$-tensor of the simulation can be rotated relative to the $\mathbf{g_1}$-tensor by specifying a set of Euler angles.[18]

The simulations are generated with careful consideration of all intensity factors, both theoretical and instrumental. This allows direct comparison of simulated spectra to the absolute intensity scale of the experimental spectrum having a known sample concentration. The only unknown factor relating the spin concentration to signal intensity is an instrumental factor that depends on the microwave detection system. However, this factor is determined by the spin standard, CuEDTA, for which the copper concentration was accurately determined from plasma emission spectroscopy.

Results

X-band (9.6 GHz) EPR spectra of HAO as isolated are shown in Figure 1 (dashed lines). For Figure 1A, the microwave magnetic field $\mathbf{B_1}$ is the conventional perpendicular orientation with respect to the static field $\mathbf{B}$, whereas for Figure 1E these two fields are parallel. Here, we present quantitative simulations of the data which allow deconvolution of the spectra and identification of four distinguishable paramagnetic species. The signal at $g = 4.3$ is from an Fe(III) impurity with a concentration of 3% of the monomer concentration. The signals from HAO do not change in shape for samples 10-fold lower in concentration than that of Figure 1.

The spectrum in Figure 1A has a set of resonances at $g = 1.35$, 2.2, and 3.1, which are values typical of low-spin ferric heme complexes. The direction corresponding to the highest g-value for low-spin heme complexes is usually approximately normal to the heme plane, and so we will refer to this spectral feature as the g_z component. The inset of Figure 1 shows an enlarged section of the experimental spectrum in A overlaid on a spectrum of a sample of HAO poised at a potential of +135 mV. At this potential only the highest potential heme of HAO ($E_m = +288$ mV) is reduced.[19] Upon reduction of that heme, the EPR signal at $g_z = 3.10$ sharpens and shifts to $g_z = 3.03$. This signal is a useful indicator of the fully oxidized state of HAO. As isolated the enzyme sometimes shows a shift toward the sharper signal at $g_z = 3.03$. Samples treated with ferricyanide consistently show the $g_z = 3.10$ feature of Figure 1. The sample

(14) Andersson, K. K.; Kent, T. A.; Lipscomb, J. D.; Hooper, A. B.; Münck, E. *J. Biol. Chem.* **1984**, *259*, 6833−6840.

(15) Andersson, K. K.; Babcock, G. T.; Hooper, A. B. *Biochem. Biophys. Res. Commun.* **1991**, *174*, 358−363.

(16) Petasis, D.; Hendrich, M. P. *J. Magn. Reson.* **1999**, *136*, 200−206.

(17) Bencini, A.; Gatteschi, D. *Electron Paramagnetic Resonance of Exchange Coupled Systems*; Springer-Verlag: New York, 1990.

(18) Brink, D. M.; Satchler, G. R. *Angular Momentum*, 2nd ed.; Clarendon Press: Oxford, 1979; p 20.

(19) Arciero, D. M.; Golombek, A.; Hendrich, M. P.; Hooper, A. B. *Biochemistry* **1998**, *37*, 523−529.

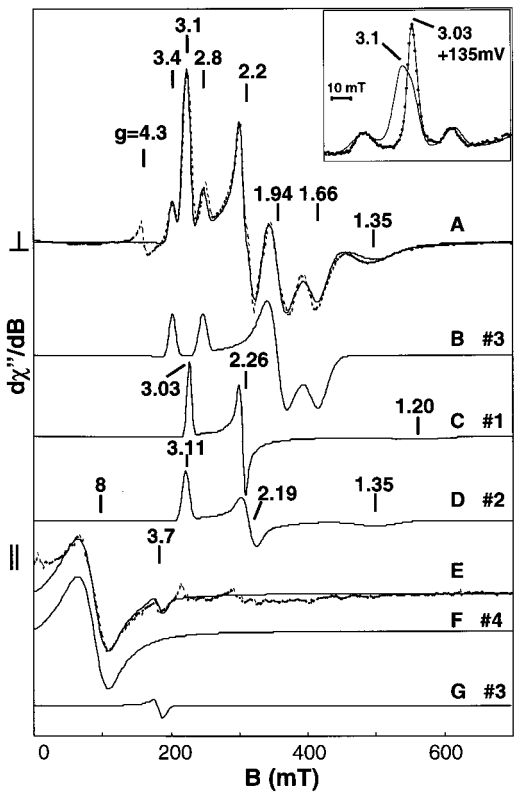

Figure 1. EPR spectra (dashed lines) and simulations (solid lines) of 0.71 mM oxidized HAO in 50 mM KPi, pH 7. (A) Overlaid on the $\mathbf{B_1} \perp \mathbf{B}$ mode experimental spectrum is a quantitative simulation composed of a sum of EPR species 1, 2, and 3 at concentrations of 0.59, 2.22, and 0.74 mM. The individual spectra of the species plotted at equal concentration are shown in (B) species 3, (C) species 1, and (D) species 2. (E) Overlaid on the $\mathbf{B_1} \parallel \mathbf{B}$ mode experimental spectrum is a quantitative simulation composed of a sum of EPR species 3 and 4 both at concentrations of 0.74 mM. The individual spectra of these species are shown in (F) species 4 and (G) species 3. Species 3 contributes intensity to signals in both microwave modes. See Table 1 for assignments and simulation parameters. Experimental conditions: (A) $\mathbf{B_1} \perp \mathbf{B}$, microwaves, 0.2 mW at 9.62 GHz, $T = 10$ K; (E) $\mathbf{B_1} \parallel \mathbf{B}$, microwaves, 0.2 mW at 9.26 GHz, $T = 2$ K. The signal gain in part E is five times that of A. The inset shows the change in the $g = 3.1$ signal for HAO poised at +135 mV (dotted line) relative to oxidized protein (solid line). The small signal at $g = 3.1$ in part E is due to imperfect alignment of $\mathbf{B_1} \parallel \mathbf{B}$.

of HAO used for Figure 1 showed no signal changes from HAO upon treatment with ferricyanide. For this sample all hemes of HAO are in the Fe^{3+} state and we will refer to this state of the enzyme as fully oxidized. Least-squares fitting of the experimental spectra of fully oxidized HAO indicates that the resonances at $g = 1.35$, 2.2, and 3.1 can be resolved into at least two different mononuclear heme species. The signals of species 1 and 2 are simulated in Figure 1, parts C and D, respectively, and the *g*-values are given in Table 1. The crystal field parameters are also given in Table 1, and both sets are typical of values for bis-His coordination to the hemes.

The set of resonances in Figure 1A at $g = 1.66$, 1.94, 2.8, and 3.4 have frequency-dependent *g*-values, which for $S = {}^1/_2$ spin centers is indicative of a spin-coupled system. Figure 2 shows spectra of HAO at four different microwave frequencies which are plotted on an equivalent *g*-scale ($g = h\nu/\beta B$). The resonances at $g = 1.66$, 1.94, 2.8, and 3.4 in Figure 2C shift with frequency. We will first treat the X-band data of Figure 1 and return to the multifrequency data later in the results. In our previous work, we could not determine the contribution from the exchange interaction between the hemes.[10] We are now able to perform simulations of the spectra which include contributions from both dipolar and exchange terms. The simulation shown in Figure 1B is calculated from eq 1 with an exchange-coupling between an equivalent pair of $S = {}^1/_2$, low-spin ferric hemes. The parameters of the simulation are listed in Table 1 for species 3. The crystal field parameters calculated from the **g**-tensor are typical of values for bis-His coordination to the heme. A simulation fit to the data requires a rotation of the $\mathbf{g_2}$-tensor of eq 1 for one heme relative to the $\mathbf{g_1}$-tensor of the other heme. The Euler rotation set for the simulation is (α, β, γ) = (45°, 180°, 135°). This set of angles is equivalent to a rotation of one heme by 180° about an axis which bisects the g_x and g_y axes. Thus, the g_z axis of the hemes remains parallel and the g_x and g_y axes are interchanged. From the temperature dependence of the signal, the isotropic exchange coupling between these two hemes is approximately $J \approx +1$ cm^{-1} (antiferromagnetic). Additional information regarding the exchange interaction for this species and the uniqueness of the fits will be given below from an analysis of the multifrequency experimental spectra.

We have developed our simulation software such that absolute determinations of signal intensities are calculated and compared directly to the experimental data. Thus, all data and simulations shown in Figure 1 are plotted on a known intensity scale. The concentration of the protein determined spectrophotometrically for this sample was 0.71 mM. The least-squares fit to the data determines the concentrations of each species necessary for the best fit to the experimental spectrum. The simulation overlaid on the data of Figure 1A (solid line) is created from a summation of species 1, 2, and 3 with concentrations of 0.59, 2.22, and 0.74 mM, respectively, where the value for species 3 is per dimer. Using the protein concentration, these signals account for 0.83, 3.13, and 2.08 hemes per monomeric subunit of HAO, respectively. Thus, the HAO EPR signals for $\mathbf{B_1} \perp \mathbf{B}$ (Figure 1A) account for a total of 6 heme centers per subunit as listed in Table 1. The simulation matches the data quite well; it is not possible to achieve such a fit with a different total number of hemes.

As expected, the EPR signals of the sample poised at +135 mV (inset, Figure 1) with $g_z = 3.4$, 3.03, 2.8 account for 5 hemes in the ratio 1:3:1. The heme with $E_m = +288$ mV has been reduced to a $S = 0$ state and no longer gives an EPR signal. However, it is not possible to simply remove one heme species from the $g = 3.1$ signal prior to reduction and obtain the $g = 3.03$ signal. The reduction of the +288 mV heme apparently causes conformational changes to the protein which affect the three other hemes of EPR species 1 and 2. Thus, the EPR assignment of the +288 mV heme is ambiguous.

The spectrum of HAO for $\mathbf{B_1} \parallel \mathbf{B}$ (Figure 1E, dashed line) shows two signals which originate from two different spin systems. The weaker signal at $g = 3.7$ originates from species 3. The simulation shown in Figure 1G uses the same parameters as that of Figure 1B, except that the simulation is now for $\mathbf{B_1} \parallel \mathbf{B}$. The simulation matches the data in both position and intensity with no adjustable intensity factors.

The larger signal near $g = 8$ for $\mathbf{B_1} \parallel \mathbf{B}$ has been previously assigned to an integer-spin state of an additional pair of exchange-coupled hemes. The simulation for species 4 is shown in Figure 1F and is the same as that published previously.[10] The isotropic exchange interaction between these hemes is $J \geq 1$ cm^{-1}. The sum of spectra F and G is overlaid in Figure 1E (solid line) and gives a quantitative match to the experimental data. Cyanide has been shown to be an inhibitor of substrate

Table 1. Properties of the Hemes of HAO

species	Fe count	hemes	E_m, mV	**g**-tensor[a]	Δ/λ[b]	V/Δ	J,[c] cm^{-1}
1	1			1.20, 2.26, 3.03	−2.27	−0.71	
2	3			1.35, 2.19, 3.11	−2.73	−0.90	
3	2	3, 5	∼0, ∼0	1.27, 2.28, 3.06	−2.39	−0.73	1[d]
4	2	P460, 6	−260, −190	8[e]			≥1

[a] The order of the **g**-values is assumed to be g_x, g_y, g_z. [b] Crystal-field parameters of the improper coordinate system.[20] [c] Isotropic value of the exchange interaction. [d] Euler rotation (α, β, γ) of $\mathbf{g_2}$ relative to $\mathbf{g_1}$ is 45, 180, 135°. $\mathbf{D'} = -0.025, -0.025, +0.05$ cm^{-1}, $\mathbf{d} = +0.01, -0.01, -0.21$ cm^{-1}. [e] Observed **g**-value of the integer-spin signal.

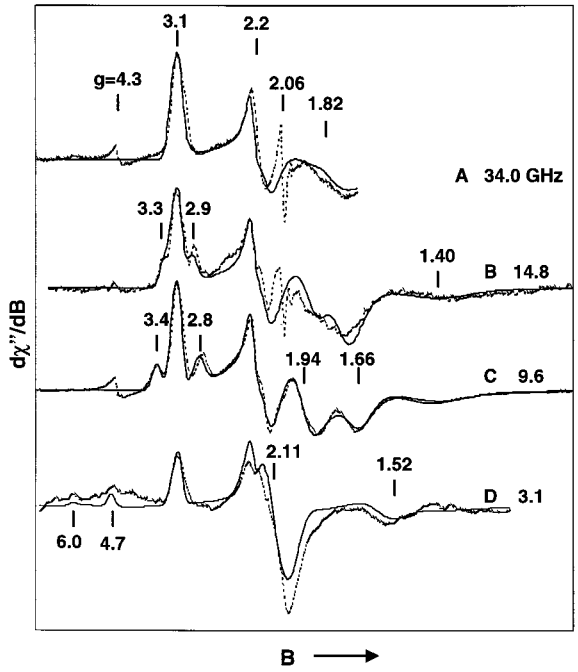

Figure 2. Multifrequency EPR spectra (dashed lines) of oxidized HAO plotted on an equivalent *g*-scale. The simulations (solid lines) all use the same parameter set as Figure 1A. The microwave frequencies are as listed in GHz; temperature, ∼10 K.

oxidation in HAO.[11] All signals for $\mathbf{B_1} \perp \mathbf{B}$, and the $g = 3.7$ signal for $\mathbf{B_1} \parallel \mathbf{B}$, are not affected by cyanide addition, whereas the $g = 8$ signal is lost upon addition of cyanide, indicating that this signal originates from heme P460 at the active site HAO.[10]

To summarize thus far, we have shown that all eight hemes per monomer of fully oxidized HAO can be quantitatively assigned to four distinguishable EPR species. As listed in Table 1, no spin−spin interaction is detected for four hemes of HAO: two hemes are exchange-coupled with $J \approx 1$ cm^{-1} and two hemes at the active site are exchange-coupled with $J \geq 1$ cm^{-1}.

Multifrequency EPR Spectra. An important test of the validity of the simulations comes from simultaneous fits to multifrequency EPR spectra. Figure 2 shows EPR spectra (dashed lines) of oxidized HAO at 34.0, 14.7, 9.6, and 3.1 GHz all with $\mathbf{B_1} \perp \mathbf{B}$. The magnetic field scale for each spectrum has been adjusted to align the *g*-value scales ($g = h\nu/\beta B$). The spectra are taken from four different preparations of HAO. The signals at $g = 4.3$ and 2.06 are from impurity species of Fe^{3+} and Cu^{2+}, respectively, which vary in amount for the different samples. The apparent truncation of Figure 2A is due to the maximum magnetic field limit of the spectrometer.

The simulations (solid lines) overlaid on the experimental spectra in Figure 2 all use the same parameter set as that of Figure 1A for all three species. The data in Figure 2A,C are obtained from instrumentation in our laboratory and are both quantitatively accurate in intensity for the protein concentration. The ratio of the amounts of the three species from least-squares deconvolution of the spectra is found to independently agree at all microwave frequencies. This match to complicated multicomponent spectra at multiple frequencies is relatively rare. In particular, the additional data at multiple frequencies require the introduction of anisotropic and antisymmetric components to the exchange interaction and we will comment on these details as we describe the spectra in the following.

The dominate features in the spectra of Figure 2 at $g = 1.4$, 2.2, and 3.1 are from the four noninteracting hemes. Attempts to simultaneously fit these features with fewer than two species gave unsatisfactory fits to the data. We also attempted to least-squares fit the data with two species, allowing g_y and g_z of both species to vary independently, but constraining g_x to the value determined by the normalization condition of the wave functions within the Griffith model of low-spin hemes.[20b] This also resulted in unsatisfactory fits to the data. The normalization condition may not be obeyed if contributions from covalency effects or higher excited states are important.

The frequency-dependent features in the spectra of Figure 2 originate from species 3 which is one of the diheme clusters. The g_z features near 3.1 for this pair of hemes are unresolved at 34 GHz, but split out as the microwave frequency is lowered. The resonance at $g = 1.82$ is from a combination of the heme in-plane *g*-values and this features also splits as the frequency is lowered. The spin Hamiltonian parameters of eq 1 for this species were determined from simultaneous least-squares fits to the multifrequency spectra. The specific simulations obtained for species 3 are shown in Figure 3 using the parameter set given in Table 1. This pair of interacting $S = {}^1/_2$ hemes is exchange-coupled to give total spin states of $S = 0$ and 1. An energy level diagram of the spin states is shown in Figure 4 for **B** along the *z*-axis.

The observed transitions are from the $S = 1$ multiplet approximately 1 cm^{-1} above the $S = 0$ state. The resonance positions are not affected by the magnitude of *J*, but are strongly dependent on the exchange anisotropy, $\mathbf{D'}$. The anisotropy splits the $|1, \pm1\rangle$ and $|1, 0\rangle$ levels in zero-field. From the fits to the data of Figure 2, we find $D'_{xx} = D'_{yy} = -0.025$, $D'_{zz} = +0.05$ cm^{-1}, and no significant off-diagonal values. The splitting of the g_z feature centered at 3.1 is clearly observable in the spectra and is due to this anisotropy. These features are from the bold transitions noted in Figure 4. The splitting increases as the microwave frequency is lowered. At 3.05 GHz in Figure 2, the low-field transition is at $g = 4.7$ and the high-field transition has merged with the resonances from the in-plane **g**-tensor components. In addition, a new resonance is observed at $g = 6.0$ which is the $|1, +1\rangle$ to $|1, -1\rangle$ transition noted in Figure 4.

(20) (a) Blumberg, W. E.; Peisach, J. in "Probes of Structure and Function of Macromolecules and Membranes"; Chance, B., Yonetani, T., Mildvan, A. S., Eds.; Academic Press, New York, **1971**, Vol. 2, pp 215−229. (b) Palmer, G. in "Physical Methods in Bioinorganic Chemistry"; Que, L., Jr., Ed.; University Science Books, Sausalito, 2000; pp 121−185.

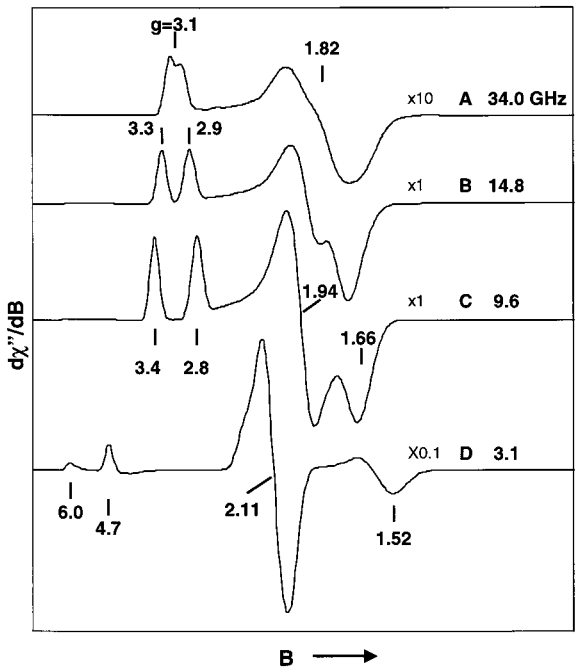

Figure 3. Simulations of EPR species 3 plotted on an equal *g*-scale. The parameters are the same as that of Figure 1B. The microwave frequencies in GHz and relative intensities are as listed.

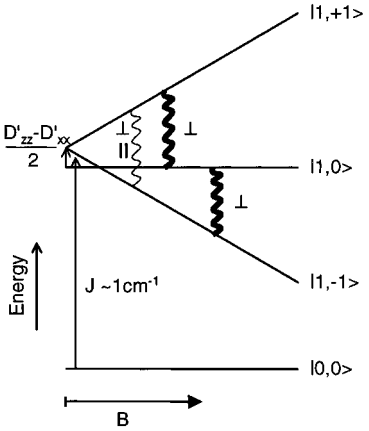

Figure 4. The energy level diagram for an antiferromagnetic exchange-coupled pair $S_1 = S_2 = {}^1/_2$. The anisotropic contribution to **J** is **D′** of eq 1, which splits the $S = 1$ spin manifold in zero-field. The allowed and weakly allowed transitions and B_1 polarization are noted.

This transition also gives the weak parallel mode signal of Figure 1G. Since X-band (9.6 GHz) spectrometers are most common, we show spectral simulations for various values of $D'_{zz} - D'_{xx}$ ($D'_{xx} = D'_{yy}$) in Figure 5. For HAO, this value is $D'_{zz} - D'_{xx} = 0.08$ cm^{-1}, which gives observed *g*-values of 3.4 and 2.8. It is possible that signals from other proteins containing this heme pair motif will show signals similar to one of the spectra of Figure 5. In complicated spectra, the shift toward higher *g*-values of the lowest field transition might be misinterpreted as an indication of the presence of a highly anisotropic low-spin heme, rather than an exchange-coupled pair of hemes.

The simultaneous fitting to the spectra of all four frequencies also requires an antisymmetric term in the exchange interaction. From the fits shown in Figure 2, we find for eq 1, $d_x = 0.009$, $d_y = -0.014$, and $d_z = -0.210$ cm^{-1}. The spectral dependency on this term is not as clearly observable as, for example, the splitting of the signals due to the anisotropic term. In particular, the spectral features at $g = 2.11$ and 1.52 for microwave

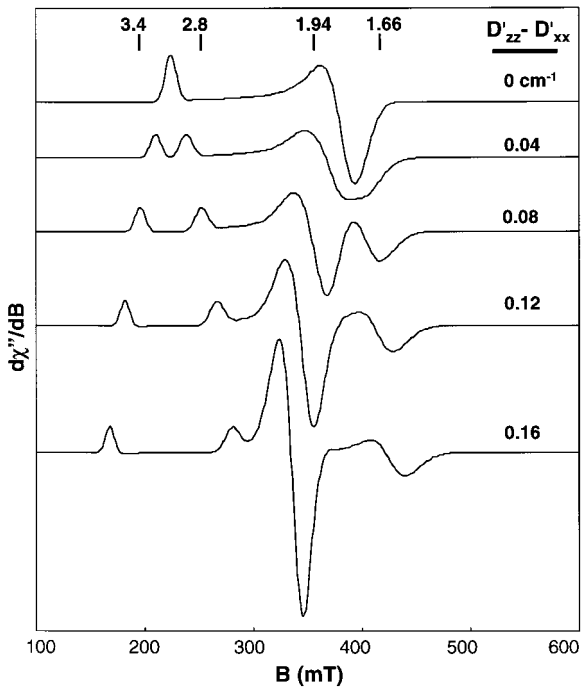

Figure 5. Simulations of EPR species 3 at 9.6 GHz showing the effect of variation of the anisotropic component of the exchange coupling, $D'_{zz} - D'_{xx}$ with $D'_{yy} = D'_{xx}$. For HAO, $D'_{zz} - D'_{xx} = 0.08$ cm^{-1}.

frequency 3.05 GHz (Figure 2D) cannot be matched without the antisymmetric term.

The additional terms in the exchange interaction clearly do not originate from a magnetic dipolar interaction. We have included a magnetic dipolar contribution into the simulation program with specification of the internuclear vector distance and spherical angles. The distances and angles used in the calculations of the dipolar interaction are taken from the crystal structure discussed later in this work. The multifrequency simulations including a dipolar term show no change in spectral features for **B** along the *z*-axis ($g \approx 3.1$). This is due to a dipolar angle that is near 54.7°, at which the dipolar contribution vanishes along the *z*-axis. Only minor effects are observed along the other axes, due to the large internuclear distance between the irons (>9 Å). The exchange terms originate from a through-bond interaction with insignificant magnetic dipolar contributions. We have also attempted to fit the data by removing the constraint of equal **g**-tensors and eliminating one or both of the anisotropic and antisymmetric exchange terms, but it is then not possible to fit the data. The anisotropic and antisymmetric exchange terms are expected for metal centers with low-lying excited orbital states and large spin−orbit interactions,[17] which is the case for low-spin heme systems.

The determinations of the exchange terms and the rotation of the **g**-tensors are dependent on different features of the spectrum. For a given value of $D'_{zz} - D'_{xx}$, the other features in the simulation are essentially determined by the rotation angle about the g_z-axis. Figure 6 shows X-band simulations as a function of the rotation angle α about the g_z-axis. For $\alpha = 0°$, the g_x and g_y axes of the two hemes are coincident. We find that the simulation fits to the data shown in Figure 2 require $\alpha = 90° \pm 5°$.

Discussion

With 24 heme centers per trimer (8 per monomer), HAO is one of the most complicated heme enzymes known. The only direct contacts between hemes are van der Waals interactions

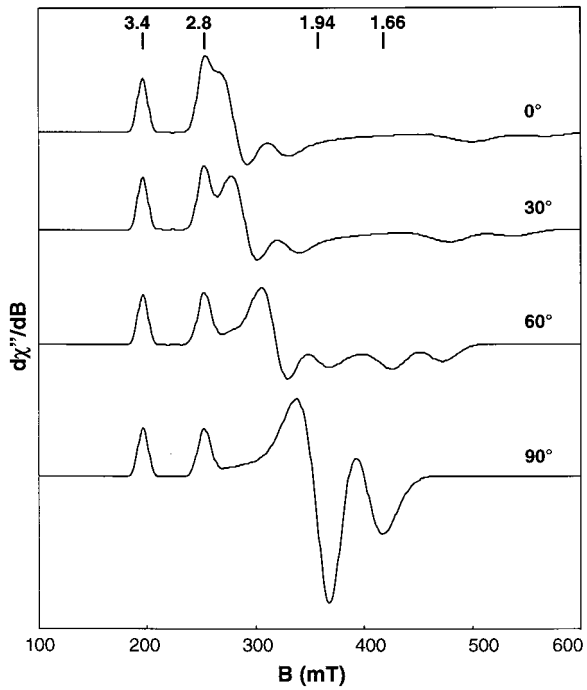

Figure 6. Simulations of EPR species 3 at 9.6 GHz showing the effect of rotation through an angle α about the *z*-axis. For α = 0°, the g_x and g_y axis of the two hemes are parallel. For HAO, α = 90°.

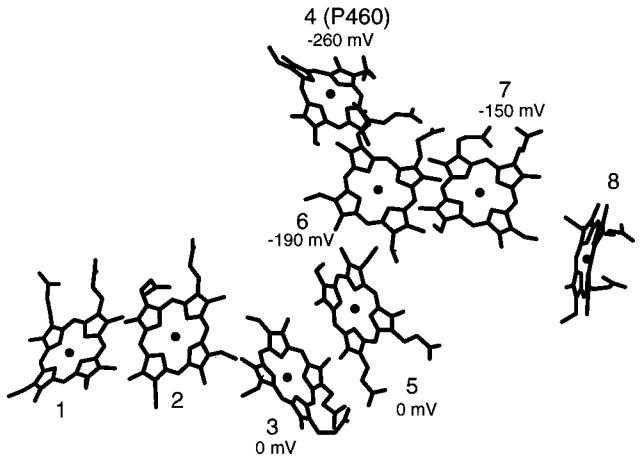

Figure 7. The heme crystal structure of a monomeric subunit of HAO. The heme numbering scheme and our assignments of various heme midpoint reduction potentials are shown.

which occur only for hemes within a subunit.[12] Thus we will simplify the system by considering only heme interactions within a subunit. The catalytic and electron-transfer processes may eventually be shown to depend on intersubunit interactions; however, no evidence currently exists for cooperativity or exchange-coupling between hemes of adjacent subunits.

HAO belongs to a growing family of structurally well-characterized bacterial multiheme proteins involved in electron-transfer and redox chemistry of small inorganic molecules. These proteins contain conserved structural arrangements of heme centers, despite significant differences in primary sequence and protein architecture. Heme organization within a subunit of HAO is comprised of a triheme cluster (hemes P460, 6, and 7), four other hemes are involved in two diheme clusters (hemes 1 and 2, and hemes 3 and 5) and one heme is not part of a cluster (heme 8). The arrangement and numbering is shown in Figure 7.[12] Closer inspection of heme organization has revealed a remarkable simplicity in that three distinct diheme packing arrangements (motifs) can be defined that account for all diheme pairings within the HAO monomer. These were first identified when the structure of cytochrome c_{554}[21] from *Nitrosomonas* was reported, and further observed in the structure of the pentaheme nitrite reductase from *Sulfurospirillum deleyianum*.[22] Two of these motifs show the porphyrins to be nearly parallel with each other but offset with only substituents on the periphery overlapping. Examples of these two motifs in HAO are heme pair 4 & 6 and heme pair 3 & 5. The third motif shows the porphyrins to be approximately perpendicular with each other. An example of this motif in HAO occurs for hemes 5 and 6. The commonality of diheme motifs within these three multiheme cytochromes has resulted in a higher order packing arrangement such that the four hemes of cytochrome c_{554} overlay spatially with hemes 3, 4 (P460), 5, and 6 of HAO, while the five hemes of NiR overlay spatially with hemes 4 (P460), 5, 6, 7, and 8 of HAO.

Despite the similarities in heme packing for the three proteins, the EPR spectrum of HAO shows moderate coupling while the EPR spectra of both cytochrome c_{554} and NiR are exceedingly complex, suggesting substantial coupling between all hemes in the latter proteins. To deconvolute these EPR spectra, we are taking the approach of seeking to describe the interactions between hemes for each of the diheme motifs so that the EPR properties of any diheme pair can be predicted. Since the diheme pairs 1 & 2, 3 & 5, and 6 & 7 are all members of the same diheme motif, we begin with an analysis of this motif. Furthermore, the split-Soret cytochrome *c* from *Desulfovibrio desulfuricans* contains a similar diheme motif.[23]

Projections of the crystal structure of heme pair 3 & 5 of HAO are shown in Figure 8. We choose a heme coordinate system which has the *z*-axis normal to the porphyrin plane, and the *x* and *y* axes along pyrrole nitrogens N1:N3 and N2:N4, respectively. These axes are labeled x_3, y_3, z_3 for heme 3 and similarly for heme 5. Heme 5 is rotated by 180° relative to heme 3 about an axis that approximately bisects the *x* and *y* axes. This rotation leaves the z_3 and z_5 axes antiparallel and inverts the x_5, y_5 axes relative to x_3, y_3. In the crystal structure, the x_5, y_5 axes are not perfectly coincident with the y_3, x_3 axes, but are offset by a rotation of 17° as noted in Figure 8. The internuclear iron vector has a length of 9.2 Å and makes an angle of 57° with respect to the *z* axes. The hemes are approximately coplanar with a vertical plane-to-plane distance of 4 Å. This heme plane inversion appears to be a consequence of heme pairs that are covalently attached to adjacent antiparallel polypeptide chains.

The electronic structure of this heme pair and its EPR spectrum can now be directly correlated to the crystallographic picture of Figure 8. Recent work by Walker and co-workers on heme model complexes has shown that the orientations of the principal components of the **g**-tensor are determined by orientation of the axial histidines with respect to the heme.[24] The g_z axis is normal to the heme plane, and the in-plane g_x and g_y axes are determined by the projection of the plane of the axial histidines onto the heme plane. For histidine planes which lie along a N−Fe−N line, the g_x axis is along this same line. As

(21) Iverson, T. M.; Arciero, D. M.; Hsu, B. T.; Logan, M. S. P.; Hooper, A. B.; Rees, D. C. *Nat. Struct. Biol.* **1998**, *5*, 1005−1012.

(22) Einsle, O.; Messerschmidt, A.; Stach, P.; Bourenkov, G. P.; Bartunik, H. D.; Huber, R.; Kroneck, P. M. H. *Nature* **1999**, *400*, 476−480.

(23) Matias, P. M.; Morais, J.; Coelho, A. V.; Meijers, R.; Gonzalez, A.; Thompson, A. W.; Sieker, L.; Legall, J.; Carrondo, M. A. *J. Biol. Inorg. Chem.* **1997**, *2*, 507−514.

(24) (a) Quinn, R.; Valentine, J. S.; Byrn, M. P.; Strouse, C. E. *J. Am. Chem. Soc.* **1987**, *109*, 3301−3308. (b) Walker, F. A.; Huynh, B. H.; Scheidt, W. R.; Osvath, S. R. *J. Am. Chem. Soc.* **1986**, *108*, 5288−5297. (c) Shokhirev, N. V.; Walker, F. A. *J. Am. Chem. Soc.* **1998**, *120*, 981−990.

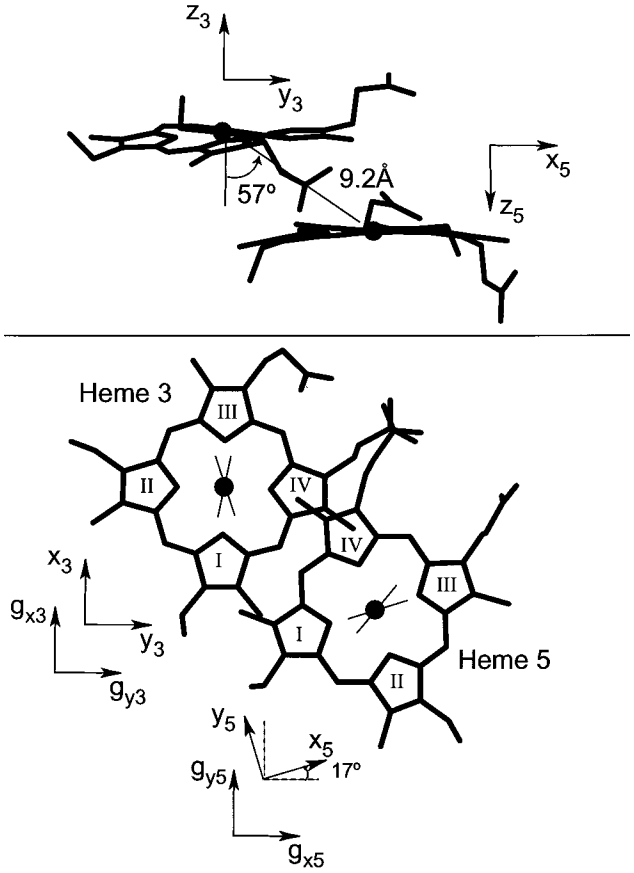

Figure 8. The structure of heme pair 3 & 5. The lower panel is a view looking down the normal to the heme planes. The upper panel is a side-on view. The axes x_3, y_3, z_3 refer to the crystallographic axes of heme 3, and similarly for heme 5. The angle between the z_3, z_5 axes is 180°, and the angle between the x_5 and y_3 axes is 17°. The thin lines on the iron atoms mark the projection of the plane of the axial histidine ligands. The g_{x3}, g_{y3} tensor axes are along the x_3, y_3 axes, whereas the g_{x5}, g_{y5} tensor axes are inverted relative to x_3, y_3 axes.

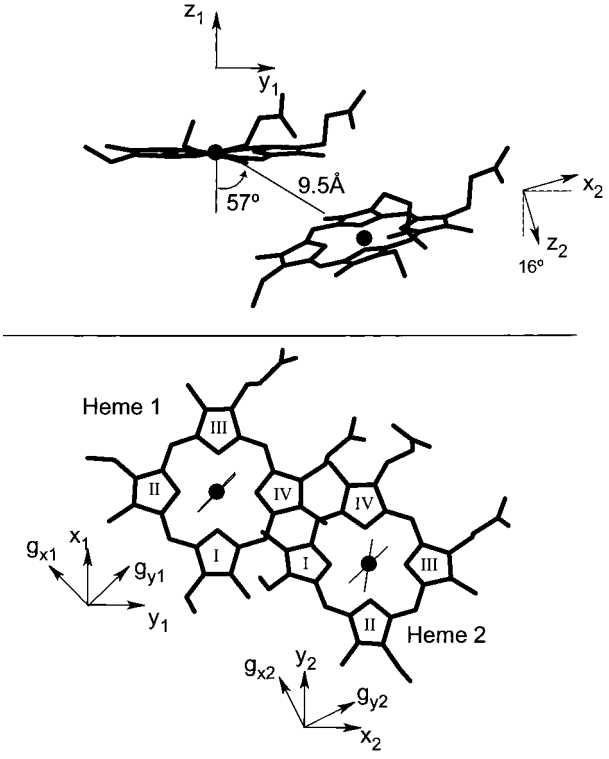

Figure 9. The structure of heme pair 1 & 2. The lower panel is a view looking down the normal to the heme planes. The upper panel is a side-on view. The axes x_1, y_1, z_1 refer to the crystallographic axes of heme 1, and similarly for heme 2. The angle between the z_1, z_2 axes is 164° and the x_1, y_1 axes are parallel to the x_2, y_2 axes. The thin lines on the iron atoms mark the projection of the plane of the axial histidine ligands. The tensor axes of both g_{x1}, g_{y1} and g_{x2}, g_{y2} are rotated by 45° relative to the x_1, y_1 axes.

the histidine planes rotate away from the N−Fe−N line, the g_x axis rotates in the *opposite* direction by the same angle. The projections of the histidine planes from the crystal structure of HAO are the thin lines on the iron in Figure 8. For heme 3, the histidine angles are 12° and −18° from x_3, and for heme 5 the angles are 33° and −3° from x_5. We assume that the average of the two histidine projections determines rotation of the electronic g_x axis.[25] The average for heme 3 is approximately 0° and the average for heme 5 is approximately 15°. Thus, as shown in Figure 8, g_{x3} is along x_3, while, due to the counter rotation, g_{x5} is nearly parallel with y_3. The resultant relative orientations of the **g**-tensors are such that g_{x3} is perpendicular to g_{x5}.

We find that the simulations for EPR species 3 match the data for the **g**-tensor orientations given in Figure 8. The simulations are both quantitative and consistent with the orientations of hemes 3 and 5. As mentioned above, heme pairs 1 & 2 and 6 & 7 have an inverted heme geometry similar to heme pair 3 & 5. In addition, while heme pair 4 & 6 have a significantly different heme alignment, the iron−iron distance is comparable to that of heme pair 3 & 5. The EPR spectra show evidence for exchange coupling for only two of these diheme clusters: EPR species 3 and 4. We make the assignments given in Table 1, namely EPR species 3 is from heme pair 3 & 5 and EPR species 4 is from heme pair 4 & 6. Our evidence for ruling out assignments to other heme pairs follows.

We have shown in previous work that EPR species 4 is associated with the active site and heme P460 (heme 4 of Figure 7).[10] This signal titrates in a 1:1 stoichiometry with cyanide, and vanishes upon treatment with peroxide which selectively destroys the P460 chromophore. The signal from species 4 must minimally originate from an exchange-coupled cluster containing heme P460 and a second half-integer spin center. This second center could possibly be a heme, the covalently linked Tyr467 if it occurs as a stable radical species, or a porphyrin radical species. Three results indicate that the second spin is a heme. First, six of the eight hemes are quantitatively accounted for by the perpendicular mode spectra, leaving two hemes for the active site exchange-coupled cluster. Second, in a reductive titration study, the $g = 8$ signal from species 4 vanishes at a midpoint potential of −150 mV and a signal at $g = 6$ from heme P460 appears at a midpoint potential of −190 mV.[19] These values do not correspond to heme P460 ($E_m = -260$ mV at pH 7), but do correspond to potentials of two other hemes. Third, the midpoint potential of the $g = 8$ signal is much lower than the typically high and positive reduction potentials of either tyrosine or porphyrin radical species. Heme 6 is the nearest spin center to heme P460, thus the exchange-coupled cluster giving EPR species 4 from HAO is heme P460 and heme 6.

For the exchange-coupled heme pair giving EPR species 3, the possible remaining assignments are heme pairs 3 & 5 or 1 & 2. The possibility that EPR species 3 is from heme pair 1 & 2 can be ruled out based on the following arguments from the structure shown in Figure 9. The orientation of heme 1 relative

(25) Bertini, I.; Luchinat, C.; Parigi, G.; Walker, F. A. *J. Biol. Inorg. Chem.* **1999**, *4*, 515−519.

to heme 2 is similar to that of hemes 3 and 5. The inversion of heme 2 relative to heme 1 leaves the x_1, y_1 axes parallel to the y_2, x_2 axes. The z_2 axis is at an angle of 16° relative to the z_1 axis. These differences do not greatly affect the EPR simulation to allow distinction from heme pair 3 & 5, however the histidine angles are significantly different and do provide a basis for distinction. The histidine angles for heme 1 are both 45° relative to x_1, and for heme 2, the angles are −9° and −45° from the y_2 axis. For these histidine angles, the expected orientations of the **g**-tensors are shown in Figure 9. In contrast to the **g**-tensors of hemes 3 & 5, the directions of g_{x1} and g_{y1} are nearly parallel with g_{x2} and g_{y2}. Simulation of the resulting EPR spectrum is shown in Figure 6 for $\alpha = 0°$. This simulation does not match the experimental spectrum even when allowing for the tilt of the g_z axes. Thus we conclude that EPR species 3 is from heme pair 3 & 5 and not from heme pair 1 & 2.

EPR species 1 and 2 originate from what are apparently four mononuclear (noninteracting) bis-histidine hemes. By elimination, these signals must originate from hemes 1, 2, 7, and 8, since the other four hemes are part of the interacting dimers. As mentioned above and shown in Figures 8 and 9, heme pairs 1 & 2 and 3 & 5 have similar structures. Why does one pair show an exchange interaction while the other pair apparently does not? For heme pair 1 & 2, the answer to this question may be due to the unique orientation of the hemes and axial histidines shown in Figure 9. If the exchange coupling between two hemes is purely isotropic and the **g**-tensors are coaxial, then the EPR spectrum from such a pair is indistinguishable from the mononuclear species. Furthermore, the parallel mode resonance for this case has vanishing intensity. Thus, hemes 1 & 2 of HAO may indeed be exchange-coupled provided the exchange coupling is isotropic. Further theoretical work which relates *g*-values and wave functions within the Griffith model to the expected exchange contributions is needed, but this is beyond the scope of the current work. It may be that symmetry arguments can rule out the presence of certain exchange terms for the case of coaxial **g**-tensors.

Our conclusions for the heme assignments are given in Table 1. From our previous potentiometric studies we are now able to correlate some of the heme potentials to the structure and these are also given in Table 1 and shown in Figure 7. EPR species 3 titrates with a midpoint potential of approximately 0 mV which correlates to the reduction potentials of two hemes determined spectrophotometrically to be approximately 0 mV. Thus, hemes 3 and 5 have midpoint potentials of approximately 0 mV. The potentials for heme P460, 6, and 7 have been previously assigned.[19] The correlation of potentials of the mononuclear hemes to the crystal structure remains ambiguous. The assignment is complicated by protein conformational changes upon reduction of the heme with $E_m = +288$ mV.

The spatial arrangement of certain hemes (e.g. heme 2 and 3) between the dimers is similar to that of the perpendicular heme arrangement observed in the tetraheme cytochrome c_3. A partial analysis of this perpendicular motif has been previously performed for one of the diheme pairs in cytochrome c_3.[26] Although the EPR spectra of most cytochrome c_3 generally do not show spin coupling between hemes, the EPR spectrum of a basic cytochrome c_3 from *Desulfovibrio africanus* has been reported to exhibit coupling.[27] We have considered the possibility of interactions between hemes 2 & 3 or 5 & 6 of HAO which exhibit a similar perpendicular arrangement. The distance between these hemes is greater than 12 Å, which results in a minimal effect in the simulations due to a magnetic dipolar interaction. From the crystal structure of HAO, the coordinate system of heme 2 is related to heme 3 by an Euler rotation of approximately (α, β, γ) = (90, 90, 45). All attempts at simulations of the data of Figure 1 with an exchange interaction and this set of Euler angles gave simulations which were clearly not correct. We have been able to simulate all signals quantitatively, and thus an interaction between these hemes in HAO is too weak to show a significant effect in the EPR spectra.

The crystal structure of HAO does not show evidence for bonds between any of the heme pairs of HAO. This is surprising given that the presence of an exchange interaction between the irons requires orbital overlap. We suspect that overlap of the porphyrin orbitals, although an edge-to-edge interaction, provides the necessary exchange pathway. The d_π orbitals of the iron have approximately 10% porphyrin character for low-spin hemes.[28] An exchange coupling of $J = 0.8$ cm^{-1} has been previously reported for a dimer complex of 5-coordinate imidazole iron octaethylporphyrin.[29] For this complex, the iron−iron distance is 4.6 Å, the separation between the parallel porphyrin cores is 3.31 Å, and one porphyrin is shifted relative to the other by 1.49 Å.[30] It would seem that this dimer structure should possess considerably more porphyrin overlap than for the hemes of HAO, and therefore the exchange interaction observed in HAO should be significantly smaller. While the HAO hemes are low-spin and thus not directly comparable, surprisingly, the exchange couplings are similar. A large exchange coupling (−139 cm^{-1}) between two V porphyrin complexes has been previously observed and attributed to an interaction between two porphyrin π cation radicals.[31] While such radical interactions are not observed in HAO, the V porphyrin study provides evidence for strong porphyrin orbital overlap between two porphyrins which are at a similar distance and have a similar relative orientation to that of the heme pairs in HAO.

Catalytic Cycle. In the catalytic cycle of HAO, NH_2OH is oxidized to HNO_2. While NH_2OH is a reasonably good reductant, the four-electron oxidation is both a unique chemical process in nature and required for growth of the organism. Two of the four equivalents are required for the primary AMO catalytic cycle, and two equivalents are utilized for respiration. The midpoint potential of heme P460 (−260 mV) is considerably more negative than that of NH_2OH (−70 mV). Thus, oxidation of substrate likely occurs after binding of NH_2OH to heme P460, rather than oxidation at an outer-sphere site. Binding of substrate to heme P460 is supported by optical and EPR data. Heme P460 and heme 6 remain oxidized in the presence of substrate, while the integer-spin EPR signal from this pair vanishes.[10] This is also evidence for the stabilization in solution of either substrate-bound complex or a bound intermediate oxidation product.

The presence of eight hemes per polypeptide chain and heme pairing appears to correlate with the unique catalytic chemistry of HAO. Heme pairs 3 & 5, 4 & 6, and possibly 1 & 2 are in direct electronic contact. These heme pairs could act as two

(26) Bertrand, P.; Asso, M.; Mbarki, P.; Camensuli, P.; More, C.; Guigliarelli, B. *Biochimie* **1994**, *76*, 524−536.

(27) Magro, V.; Pieulle, L.; Forget, N.; Guigliarelli, B.; Petillot, Y.; Hatchikian, E. C. *Biochim. Biophys. Acta* **1997**, *1342*, 149−163.

(28) (a) Zerner, M.; Gouterman, M.; Kobayashi, H. *Theor. Chim. Acta* **1966**, *6*, 363−400. (b) Weissbluth, M. *Hemoglobin*; Springer-Verlag: New York, 1974; p 133.

(29) Gupta, G. P.; Lang, G.; Scheidt, W. R.; Geiger, D. K.; Reed, C. A. *J. Chem. Phys.* **1985**, *83*, 5945−5952.

(30) Scheidt, W. R.; Geiger, D. K.; Lee, Y. J.; Reed, C. A.; Lang, G. *J. Am. Chem. Soc.* **1985**, *107*, 5693−5699.

(31) Schulz, C. E.; Song, H.; Lee, Y. J.; Mondal, J. U.; Mohanrao, K.; Reed, C. A.; Walker, F. A.; Scheidt, W. R. *J. Am. Chem. Soc.* **1994**, *116*, 7196−7203.

electron redox centers to afford a two-step, two-electron oxidation process in which HNO is an intermediate. Based on heme locations, the path of electron transfer through HAO may be from the active site, through heme pair 3 & 5, to heme pair 1 & 2. Heme 1 is the only heme with significant solvent exposure and is believed to be the donor site to the acceptor protein cytochrome c_{554}. The midpoint potentials of the hemes in HAO do not readily conform to this pathway. Only one heme has a potential more positive than hemes 3 or 5, thus hemes 1 and 2 cannot both have potentials more positive than hemes 3 and 5. However, we have observed conformation changes in the protein upon reduction of the +288 mV heme which may complicate this correlation.

The heme pairs in HAO are suspected of being a novel type of electron transport pathway in biological systems, whereby electrons move through the chain in tandem. The heme dimer structure in HAO is a motif that is appearing in a number of new structures of multiheme proteins. Such structures are likely to provide new biochemical functions in proteins, as is the case for HAO.

Acknowledgment. This research was supported by grants from the National Institute of Health (GM-49970 to M.H.) and the National Science Foundation (MCB-9723608 to A.H.).

JA002982D